Biomimetic apatite-based biomaterials: on the critical impact of synthesis and post-synthesis parameters

Nicolas Vandecandelaere, Christian Rey, Christophe Drouet

Biomimetic apatite-based biomaterials: on the critical impact of synthesis and post-synthesis parameters

Nicolas Vandecandelaere · Christian Rey · Christophe Drouet

Abstract Nanocrystalline apatites are major constituents of hard tissues, and attempts are made worldwide to prepare synthetic analogs. However the impact of synthesis/postsynthesis parameters is often disregarded. Based on an updated knowledge on such compounds, we inspected the effects of synthesis parameters (maturation time, temperature, pH, nature of counter-ions) and post-treatments (re-immersion in aqueous media, thermal treatment) on physicochemical characteristics. Great modifications were noticed during the 3 first days of maturation, where a progressive evolution of the apatite phase (localized in the core of the nanocrystals) toward stoichiometry was observed at the expense of the non-apatitic surface layer which progressively disappears. Similar trends were also evidenced for maturation run under increasing temperatures, studied here in the range 20–100 °C. pH impacted more specifically the chemical composition. The nature of the counter-ion in the starting phosphate salt influenced composition and nonstoichiometry, depending on its (in)ability to be incorporated in the lattice. Freeze-drying allowed to preserve a high surface reactivity, although further evolutions were noticed after re-immersion. Effects of a thermal treatment of dried samples were unveiled, suggesting a denaturation of the hydrated layer on the nanocrystals. This work underlines the necessity of a good control of synthesis/postsynthesis parameters for the production of biomimetic apatites.

N. Vandecandelaere · C. Rey · C. Drouet (✉)
CIRIMAT Carnot Institute, UMR CNRS/INPT/UPS,
University of Toulouse, Ensiacet 4 allée Emile Monso,
31030 Toulouse Cedex 4, France
e-mail: christophe.drouet@ensiacet.fr

1 Introduction

Calcium phosphate nanocrystalline apatites are major constituents of hard tissues in vertebrates [1]. In nature, those compounds are poorly-crystallized and depart from the stoichiometric entity, namely hydroxyapatite (HA, $Ca_{10}(PO_4)_6(OH)_2$). This is chiefly linked to the presence of ionic vacancies in calcium and in hydroxide sites and to the replacement of phosphate ions by divalent anions such as hydrogenphosphate HPO_4^{2-} or carbonate CO_3^{2-}, among other ions [2, 3], as well as (to a lesser extent) to the substitution of calcium ions by foreign elements such as magnesium or strontium. Furthermore, it has been shown that biomimetic apatites are composed of nanosized crystals which exhibit on their surface a calcium phosphate non-apatitic hydrated layer containing labile ionic species [4–10]. These species lead in particular to additional IR bands as compared to well-crystallized apatites, which can be related to non-apatitic ionic environments [11]. This updated description of biomimetic nanocrystalline apatite compounds, involving a non-apatitic phosphocalcic hydrated surface layer, thus allows one to inspect, with a renewed attention, the effect(s) of a modification of synthesis and post-synthesis parameters.

Those physicochemical features are thought to be of great biological relevance since the high ionic mobility within the hydrated layer on biomimetic apatite nanocrystals (whether of natural origin or their synthetic analogs prepared under close to physiological conditions) may explain the role of bone mineral in homeostasis (regulation of the concentration of ions and to some extent of biomolecules, in body fluids). This exceptional surface reactivity of apatite nanocrystals was indeed found to allow rapid ionic exchanges with ions from the surrounding fluids [2, 12, 13] and/or the adsorption of (bio)molecules or drug

[14]. The last decade has seen an increasing interest concerning the synthesis and exploitation of such "biomimetic" calcium phosphate, especially for bone-related applications (prosthesis coatings, filling materials/cements…), due to their remarkable bioactivity and potential resorption abilities. Indeed, biomaterials based on nanocrystalline apatites are bound to lead to (i) a better osteointegration, due to their high similarity to bone mineral, and (ii) controllable resorption properties, taking into account the higher solubility, as compared to commercially available, less-bioactive products based on stoichiometric HA or else to biphasic HA/βTCP scaffolds. Also, the possibility to tailor the physicochemical properties of such compounds, such as their chemical composition, crystalline state, morphology, surface area or porosity, among other parameters, may permit a controlled release of drugs or bioactive ions.

The preparation of synthetic calcium phosphate apatite compounds has been the object of a great number of studies, and various synthesis protocols have been tested including precipitation methods [15–17], sol–gel [18], hydrothermal synthesis [19], mechanochemical synthesis [20], vapor diffusion [21, 22], emulsion-based synthesis [23], electrospraying or electrospinning [24, 25]. However, the obtained compounds did not always exhibit similar physicochemical features to those of bone mineral, in particular in terms of hydrated and nanocrystalline characters. Among these methods, those based on aqueous precipitation in "mild" conditions appear are particularly promising. A "biomimetic" approach consists in apatite precipitation at room or physiological temperature and in the presence of an excess of phosphate ions so as to provide an inner control of pH close to the physiological value, without the need of external buffers.

In all cases, the selection of synthesis parameters should be seen as fundamental, as protocol modifications may lead to significant changes of the physicochemical characteristics of the obtained compounds. Samples prepared by neutralization of H_3PO_4 by $Ca(OH)_2$ at varying temperatures [26] were found for example to exhibit different degrees of crystallinity and hydration. The impact of maturation time in solution and pH were also preliminarily evidenced in previous works [6, 27].

However, the role of synthesis and post-treatment parameters is often not fully considered or underestimated in literature studies, and may also be disregarded in industrial developments and production. In this contribution, we demonstrate that such parameters play in fact a key role in obtaining and controlling specific physicochemical characteristics for nanocrystalline apatites. Furthermore, we point out that a fine characterization through complementary methods is necessary for precisely identifying the phase(s) in presence and unveil their potential evolutions. We followed here the effects of various synthesis parameters (maturation time in solution, temperature, pH, nature of counter-ions) and post-synthesis treatments (re-immersion in aqueous media, thermal treatment) on the physicochemical features of nanocrystalline apatites, and we show that their control is essential for the obtainment of well-defined biomimetic apatite-based bioceramics intended for bone tissue engineering.

2 Materials and methods

2.1 Nanocrystalline apatite synthesis: reference protocol

In the standard case, the synthesis of nanocrystalline calcium phosphate apatite was obtained here through a biomimetic-like approach, allowing the precipitation of biomimetic apatite in aqueous medium, at room temperature and physiological pH. The precipitation methodology involved a source of calcium ions and a source of phosphate ions. Namely, a calcium-containing solution (solution A, 750 ml) was prepared by dissolving calcium nitrate $Ca(NO_3)_2{\cdot}4H_2O$ (Merck Emsure grade, purity $\geq$99.0 %) in deionized water, up to reaching the concentration of 0.3 M. In parallel, solution B (1500 ml) containing a phosphate source was prepared by dissolving di-ammonium hydrogenphosphate $(NH_4)_2HPO_4$ (VWR Normapur grade, purity $\geq$99.0 %) up to the concentration of 0.6 M. Solutions A and B were mixed, at ambient temperature and under stirring for 5 min, and then left to mature in the precipitating medium for 1 day (aging in solution). The precipitating medium was then separated into four equal subparts, filtered on Büchner funnels, thoroughly washed with deionized water (4 L per funnel), and freeze-dried for 3 days (freeze-dryer set to −80 °C and residual pressure 10 mbar). During this whole synthesis protocol, the reaction medium was buffered at a pH value close to the physiological one (pH ~7.2) thanks to the presence of a large excess of phosphate ions; this excess being defined relatively to the hydroxyapatite precipitation reaction:

$$10Ca(NO_3)_2 + 6(NH_4)_2HPO_4 + 2H_2O \rightarrow Ca_{10}(PO_4)_6(OH)_2 + 12NH_4NO_3 + 8HNO_3$$

Unless otherwise mentioned, the freeze-dried precipitate powder was then collected and stored in a freezer at −18 °C prior to physicochemical analyses.

2.2 Modifications of synthesis parameters

In order to follow the potential influence of a modification of synthesis parameters on the physicochemical characteristics of the obtained compound, several tests were

carried out with modified synthesis parameters as compared to the previously described "reference" synthesis protocol. Namely, modified parameters are:

- the maturation time in solution, i.e. the time frame spent between the beginning of the precipitation and the end of the washing step, studied in the range 20 min–20 days (20 min, 6 h, 15 h, 1, 3, 6 and 20 days).
- the maturing temperature: ambient temperature (20 °C), physiological temperature (37 °C), 50 and 100 °C.
- the maturing pH, forced to pH values of 6, 8, 9, 10 or 11 by addition of either concentrated ammonia or nitric acid (VWR Normapur grade, purity ≥99.0 %), as needed.
- the nature of the counter-ion in the starting phosphate salt: di-ammonium hydrogenphosphate $(NH_4)_2HPO_4$ or di-sodium hydrogenphosphate Na_2HPO_4 (Merck grade Emsure, purity ≥99.0 %).

2.3 Post-treatments

The influence of several post-treatments on the potential evolution the apatitic phase was also checked. The tested post-treatments are the following:

- immersion of the produced powder into several media buffered at pH 7.2: deionized water (brought to pH 7.2 by addition of sodium hydroxide), a phosphate-containing aqueous solution (di-ammonium hydrogenphosphate, 0.6 M), the retrieved precipitating medium.
- thermal treatment of apatite powder in an oven during 3 days at 37, 50 or 100 °C.

When mentioned in the text, magnesium-calcium surface ion exchanges were carried out on the apatite samples, at room temperature, by soaking the (initially calcium-rich) samples in a solution containing Mg^{2+} ions at a concentration of 1 M and using a constant solid-to-liquid ratio (200 mg powder in 50 ml solution). The duration of the immersion in the exchange solution was set to 12 min (2 min under stirring and 10 min static). This protocol was indeed found previously to lead to a stabilized amount of exchanged Mg^{2+} ions and, in these conditions, only surface Ca^{2+} ions were found to undergo an exchange with magnesium ions [13].

2.4 Physicochemical characterization

The nature and crystallographic structural features of the crystalline phases obtained in this work were investigated by X-ray diffraction (XRD) on a Seifert θ–2θ XRD 3000 TT diffractometer using the Cu $K_{\alpha 1}K_{\alpha 2}$ radiation (with $\lambda_{K_{\alpha 1}Cu} = 1.54051$ Å and $\lambda_{K_{\alpha 2}Cu} = 1.54433$ Å). The acquisition time was set to 60 s with a step of 0.04°, and the recorded 2θ range was 22–58°. The XRD patterns were treated by full profile fitting using the JANA 2006 software. The diffraction peaks were fitted as pseudo-Voigt curves with unfixed Gaussian–Lorentzian proportions, allowing the system to be anisotropic [anisotropic particle broadening, direction (001)]. Stoichiometric HA, crystallizing in the $P6_3/m$ space group (hexagonal), was chosen as reference material (unit cell parameters a = b = 9.418 Å and c = 6.884 Å). The profile fitting was run after subtraction of a 5-points baseline spreading throughout the whole pattern. Each experimental XRD pattern was fitted five times for determination of mean values and standard deviations. Mean crystallite dimensions (length along the c-axis and mean width) were estimated using Scherrer's formula, from the analysis of the (002) and (310) peak widths respectively. The crystallite mean length could also be derived applying Hosemann and Vogel's model [28] to the (002) and (004) planes, taking into account the plausible existence of crystal disorder effects.

For complementary identification, Fourier transform infrared (FTIR) spectra were recorded on a Nicolet 5700 spectrometer, using the KBr pellet method, in the range 400–4,000 cm^{-1} (64 scans, resolution 4 cm^{-1}). Spectral decompositions have been carried out, after subtraction of a linear baseline, in the 400–800 cm^{-1} wavenumber range corresponding to the $\nu_2\nu_4(PO_4)$ and $\nu_L(OH)$ vibration modes of phosphate and hydroxide ions, using the ORIGIN 8.1 software. These mathematical decompositions are based on Kauppinen's methodology [29]. Previously reported data [5, 11, 30, 31] served as starting point for the positioning of each contributing band existing in this spectral domain: at 470 cm^{-1} corresponding to $\nu_2(PO_4^{3-})$, 530–534 cm^{-1} (non-apatitic HPO_4^{2-}), 550 cm^{-1} (apatitic HPO_4^{2-}), 560/575 cm^{-1}/601 cm^{-1} (apatitic PO_4^{3-}), 617 cm^{-1} (non-apatitic PO_4^{3-}), 631 cm^{-1} ($\nu_L(OH^-)$), and 670 cm^{-1} (H_2O libration mode) [32]. The bands were considered as Lorentzian in shape. Ratios of bands integrated intensities were used to follow the evolution of spectral features, taking the sum of apatitic phosphate bands as a reference. The good reproducibility of the decomposition outputs (integrated intensity of each band) for a given sample has been checked by triplicate analyses, and the reported relative intensities correspond to the mean of the three tests ± standard deviation.

The chemical composition of the samples obtained was assessed through the measurement of ionic contents. The determination of the calcium and orthophosphates (PO_4^{3-} and HPO_4^{2-} ions) contents were obtained, after dissolution of the samples in perchloric acid by way of EDTA complexometry and visible spectrophotometry (using the

phoshpho–vanado–molybdenic complex, with $\lambda = 460$ nm), respectively [33]. The Ca/P atomic ratio of apatites was calculated from the result of these two analyses. The relative uncertainty on calcium and phosphorus concentrations has been evaluated at 0.5 %. When sodium-containing salts were used (as indicated in the text), sodium contents in the solids were determined by ion chromatography using a Metrohm 761 SD compact 1C apparatus equipped with a Metrosep C2100 cationic column. The eluent used was HNO_3 2 mM. When magnesium was present in the samples (after surface ion exchange), the Mg^{2+} content was assessed by atomic absorption (Perkin Elmer A-Analyst 300) after dissolution of the apatite sample in perchloric acid. When appropriate, the carbonate content of the apatite samples was derived from coulometry analyses (UIC Coulometrics), based on the measured extent of CO_2 released upon acidic treatment.

3 Results and discussion

3.1 Nanocrystalline apatite sample obtained by the "reference" synthesis protocol

In a first stage, the physicochemical characteristics of the sample obtained through the so-called "reference" synthesis protocol described in the above section were investigated, as a starting point of this study. The XRD pattern corresponding to the powder obtained after freeze-drying is given in Fig. 1, in comparison to the case of (sintered) stoichiometric HA.

As can be seen, the diffraction peaks observed can all be indexed in the apatitic structure (hexagonal, $P6_3/m$ space group) and no trace of secondary crystalline phase was detected. It may however be inferred that the crystallinity state of the sample prepared by this "reference" biomimetic-like synthesis route is significantly low, as evidenced by the width of the diffraction peaks, and this low crystallinity is also a specific feature of biological apatites found in bone or dentin for example. Profile-fitting analysis allowed us to estimate the unit cell parameters a $\sim$ 9.437 $\pm$ 0.004 Å and c $\sim$ 6.871 $\pm$ 0.002 Å. These findings indicate a greater value for the "a" unit cell parameter and a smaller value for the "c" unit cell parameter as compared to (sintered) stoichiometric HA. This contraction of the apatite unit cell along the c-axis and expansion along perpendicular directions is generally observed in the case of nonstoichiometric apatite compounds [34].

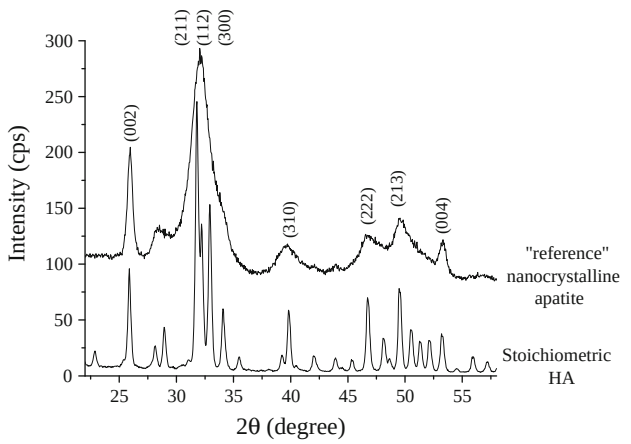

Fig. 1 XRD pattern of biomimetic nanocrystalline apatite obtained by the "reference" synthesis protocol and of stoichiometric HA

The full width at half maximum (FWHM) of the peaks relative to the (002) and (310) planes were then exploited to derive the mean crystallite dimensions, respectively in terms of length (along the c-axis) and mean width. Evaluations drawn from application of Scherrer's formula led to a length close to 19.4 $\pm$ 0.1 nm and a mean width close to 3.5 $\pm$ 0.1 nm. These values therefore confirm the nanocrystalline character of the apatite sample thus obtained. The model proposed by Hosemann and Vogel [28] was however also applied [to the (002) and (004) lines belonging to the common family of diffracting planes (00 *l*)] to re-estimate the mean length of the crystallite while taking into account the existence of constrains within the nanocrystals (crystal disorder). In this case, this "corrected" mean length could be estimated to 14.5 $\pm$ 0.2 nm. This slightly lower value, as compared to the one evaluated from Scherrer's formula, thus tends to unveil the existence of intrinsic crystal microstrains [35, 36], which is rather unsurprising for nanocrystalline apatites that are generally found to exhibit in particular a non-negligible amount of ionic vacancies and/or ionic substitutions. The associated disorder parameter (often referred to as "$g_{(002)}$") was then evaluated to 0.0070 $\pm$ 0.0002.

TEM observations (Fig. 2) enabled us to confirm the nanosize of the constitutive crystals, and a homogeneous plate-like crystal morphology was found throughout the observed specimen, as is also the case for biological nanocrystalline apatite crystals [37].

Ion content determinations led, for 100 mg of sample, to a calcium content of 0.866 $\pm$ 0.005 mmol and an orthophosphate content of 0.592 $\pm$ 0.003 mmol; giving a Ca/P mole ratio of 1.46 $\pm$ 0.02. It can be noted that this value is significantly lower than the Ca/P ratio of hydroxyapatite (1.67) therefore stressing the nonstoichiometric character of this apatite compound.

As recalled in Sect. 1, in the case of calcium phosphate apatites, such a nonstoichiometry (observed also for biological apatites arising from bone or dentin) is generally accompanied by the presence of a non-apatitic calcium phosphate hydrated layer on the surface of the nanocrystals. In order to shed some light on this matter, the spectral

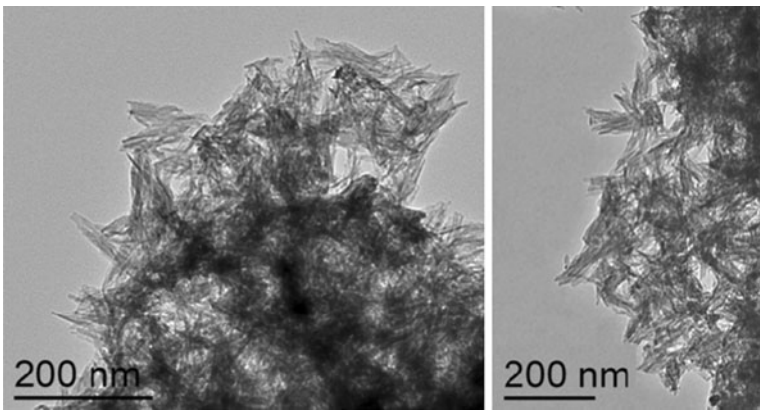

Fig. 2 TEM micrograph for biomimetic nanocrystalline apatite obtained by the "reference" synthesis protocol

decomposition of the FTIR vibration domain corresponding to the 400–800 cm^{-1} wavenumber range (hosting the $\nu_2\nu_4(PO_4)$ and $\nu_L(OH)$ vibration modes of phosphate and hydroxide ions respectively) has been achieved. Figure 3 shows the decomposition result based on the decomposition method detailed in Sect. 2.

As expected from previous studies [5, 11, 30, 31], besides the absorption bands related to PO_4^{3-} ions localized in apatitic chemical environments, the presence of HPO_4^{2-} ions in both apatitic and non-apatitic environments can be assessed by the high relative intensity of bands at 550 and 530 cm^{-1}. The band at 617 cm^{-1} generally attributed to non-apatitic PO_4^{3-} ions appears also in the decomposition, but only as a very weak band. The band at 631 cm^{-1} attributable to (apatitic) OH^- ions is clearly detectable, although its relative intensity is significantly lower than in the case of HA. This last observation as well as the detection of a noticeable amount of HPO_4^{2-} ions thus confirm the departure from stoichiometry of the apatite sample obtained by the "reference" synthesis protocol, which agrees well with the XRD and compositional data reported above. A librational water band at 670 cm^{-1} is also noticed for this "reference" nanocrystalline apatite sample, which may be linked to surface water molecules remaining after freeze-drying [32].

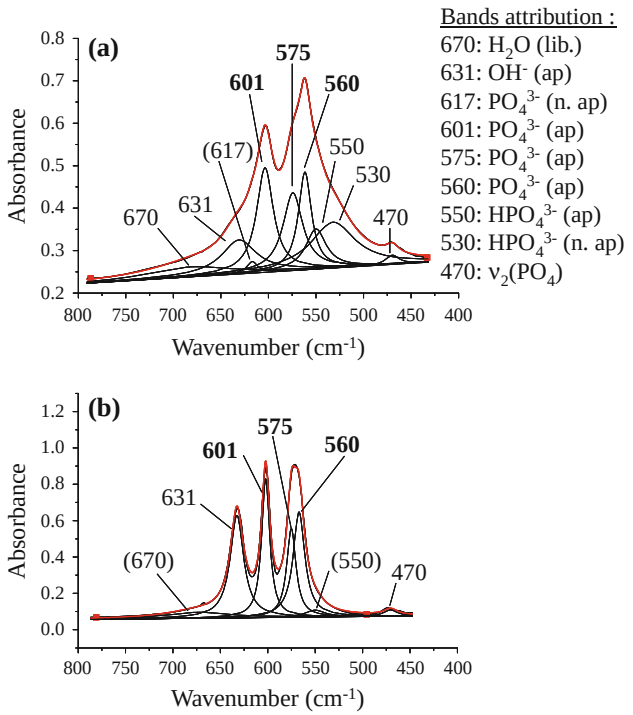

Fig. 3 Spectral decomposition of FTIR 400–800 cm^{-1} vibration domain **a** for biomimetic nanocrystalline apatite obtained by the "reference" synthesis protocol and **b** for stoichiometric HA

All the above results thus give an overview of the main physico-chemical characteristics of the apatite sample obtained by the "reference" synthesis protocol. It has thus served as a basis in the following sections aimed at evidencing a potential evolution of the apatite phase upon modifications of synthesis parameters, or due to post-treatments.

3.2 Effect of synthesis parameters

3.2.1 Effect of maturation time in solution

The first synthesis parameter that was followed in this work was maturation time in solution (at room temperature), which was tested between 20 min and 20 days (20 min, 6 h, 15 h, 1, 3, 6 and 20 days).

X-ray diffraction analyses showed that all precipitated samples retained an apatitic structure with broad diffraction peaks, and no trace of secondary crystalline phase was detected (Fig. 4).

As the maturation time increased, however, the diffraction peaks were found to become thinner, which is particularly visible for lines (002) and (004), thus evidencing a modification of the phase in presence. Moreover, the XRD patterns obtained exhibited an increasingly greater resolution upon maturation, which may be especially appreciated for line (310) for example. These effects

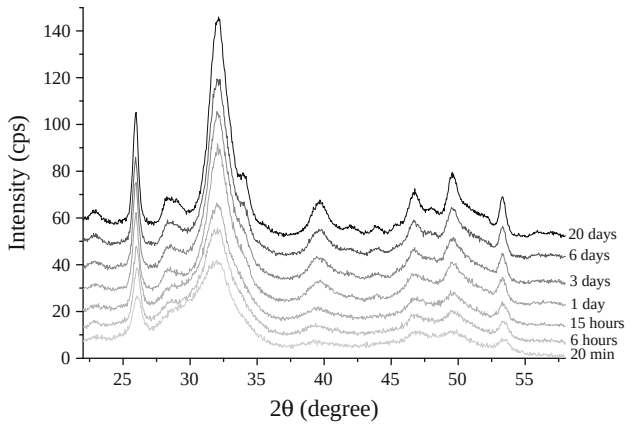

Fig. 4 Effect of maturation time (in solution) on XRD patterns of precipitated phases (room temperature)

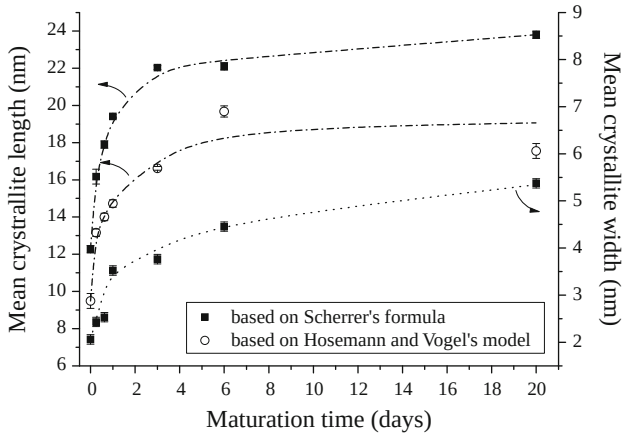

Fig. 5 Effect of maturation on estimated apatite crystallite dimensions (based on either Scherrer's or Hosemann and Vogel's models)

are bound to be due to intrinsic modifications in apatite composition/stoichiometry and/or crystallite size/internal constrains.

The application of Scherrer's formula to lines (002) and (310) led, as previously, to a first estimate of crystallite length and mean width (Fig. 5). The mean lengths and widths obtained by application of this model were in the ranges 12–24 and 2–5 nm respectively. Although these crystallites remain nanometer-sized, these findings indicate a clear increase of crystallite dimensions (with a factor close to 2), in both length and width, as evidenced here over a period of 20 days. As previously, a corrected value of the mean crystallite length could be reached with Hosemann and Vogel's model [28], leading to values ranging from 9.5 to 20.4 nm upon maturation up to 20 days. Again, these values are lower than those obtained by Scherrer's formula, which probably stresses the existence of intracrystallite strains. The existence of such microstrains is indeed supported by the evaluation of the

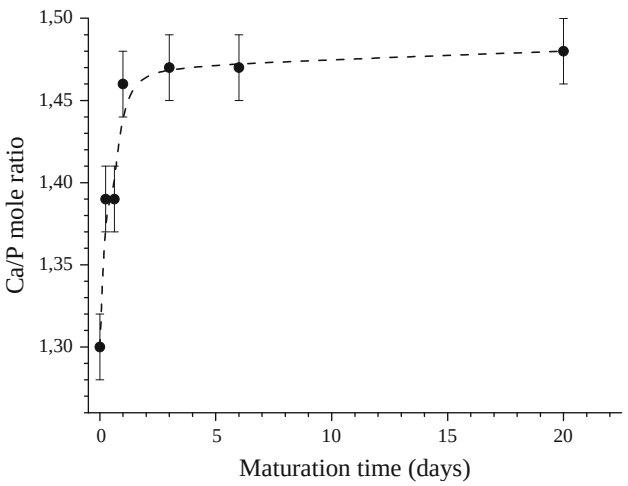

Fig. 6 Ca/P mole ratio for nanocrystalline apatites obtained for increasing maturation times in solution (at room temperature)—*error bars* represent standard experimental uncertainties

disorder parameters $g_{(002)}$, ranging from 0.0106 ± 0.0012 for 20 min of maturation to 0.0059 ± 0.0007 for 20 days. This decrease in the "g" parameter upon maturation along with the above-mentioned increase in crystallite dimensions is thus indicative of an improved crystallinity state (larger crystals exhibiting a greater overall degree of crystalline order).

Microscopy observations by TEM again confirmed the nanosized character of the crystals obtained here, independently of the maturation time. Note that it was not possible to evaluate precisely the mean crystal dimensions from TEM micrographs due to a difficulty to observe individualized crystals (strong agglomeration effect). However, the previously-mentioned plate-like morphology was conserved whatever the maturation time tested.

Chemical analyses led to an increasing value of the global Ca/P mole ratio of the samples, between 1.30 ± 0.02 and 1.48 ± 0.02 (Fig. 6), for maturation time from 20 min to 20 days. It should however be kept in mind that such values accounts for the calcium and phosphate ions that are present both in the apatitic core and within the hydrated layer, the latter being non-apatitic in nature. Therefore a direct comparison of these values to that of stoichiometric hydroxyapatite may only be considered with precautions. Such values remain however noticeably lower than 1.67 and the existence of vacancies in the apatitic core (nonstoichiometry), especially in cationic and OH sites, can most likely contribute importantly to explain these low Ca/P values. The monotonous increase of the overall Ca/P ratio, upon maturation, points out a progressive evolution of the apatite phase towards stoichiometry and/or a diminution of the hydrated layer, and this can then be related to the increased crystallinity state previously inferred from XRD analyses.

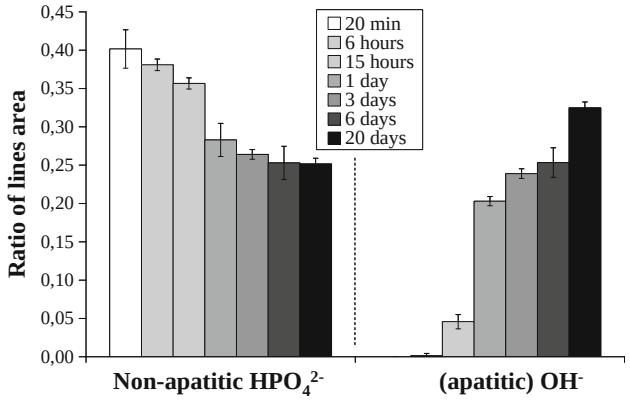

Fig. 7 Evolution of non-apatitic HPO_4^{2-} and (apatitic) OH^- ratios of *lines* area (based on FTIR decompositions) upon maturation at RT

FTIR spectral decompositions in the 400–800 cm^{-1} region, carried out as previously, enabled us to notice a progressive increase of the OH^- content (as witnessed by the increase of the relative intensity of the band at 631 cm^{-1}) as the maturation time increased. In parallel, a decrease of the relative intensity of band at 530 cm^{-1} attributed to non-apatitic HPO_4^{2-} ions was evidenced (Fig. 7). They indicate the progressive evolution of the apatite phase (localized in the core of the nanocrystals) toward stoichiometry, at the expense of the non-apatitic surface layer which progressively disappears (as witnessed by the steady decrease in non-apatitic HPO_4^{2-} ions). A more detailed analysis reveals that these evolutions are especially significant during the first 3 days or maturation, and become less pronounced beyond 3 days.

All the above results thus point out that the amount of time spent in the precipitating medium (so-called maturation time) has a direct effect on the physico-chemistry of the obtained precipitated crystals, most likely undergoing crystal growth and/or dissolution-reprecipitation phenomena. Maturation time thus appears as a key synthesis parameter that needs to be controlled so as to obtain nanocrystalline apatite samples with reproducible features. This is of particular relevance since we show here that maturation time directly affected the extent of hydrated layer (evidenced by the progressive decrease in non-apatitic ionic contents) and the degree of nonstoichiometry of the apatite phase, which are known to be two parameters conditioning the reactivity of nanocrystalline apatites. In other words, the reactivity of such apatites may potentially be tailored by modifying adequately the maturation time during synthesis. This was indeed confirmed by preliminary Mg^{2+}/Ca^{2+} surface ion exchange experiments run on such apatites, which enabled us to estimate that ca. 8.0 ± 1.0 % of the total amount of calcium ions were exchangeable for a sample matured for 20 min, as opposed to only ca. 3.5 ± 1.0 % after 20 days of maturation. In a quite similar way, the decrease of the amount of non-apatitic ions as well as an increased crystallinity was also observed for biological apatites, upon ageing [36, 38].

3.2.2 *Effect of maturation temperature*

In order to follow the potential influence of maturation temperature on the physico-chemical characteristics of the precipitated phase(s), additional maturations have been conducted, in a closed vial at 37 °C (physiological temperature), 50 and 100 °C. For this study, a constant maturation time of 1 day was used.

The XRD patterns recorded on the obtained samples showed an increased resolution of the diffraction lines as the maturation temperature increased, in a quite similar way as noticed in Sect. 3.2.1. Mean crystallite dimensions were also found to significantly increase upon heating, with mean Scherrer lengths varying from 19.4 to 43.4 nm (from 14.5 to 37.4 nm after Hosemann and Vogel's model) and mean Scherrer widths ranging from 3.5 to 10.1 nm, for maturation temperatures between 20 and 100 °C. This effect can most probably be related to a faster crystal growth, which is increasingly favored as temperature raise.

Chemical titrations enabled us to determine the Ca/P mole ratio of these samples. The values obtained (1.46 for maturation run at 20 °C, 1.50 for 37 °C, 1.54 for 50 °C and 1.58 for 100 °C) were found to increase monotonously upon temperature increase, witnessing also a progressive evolution of the apatite chemical composition towards stoichiometry. This tendency was also confirmed by FTIR spectral analyses (Fig. 8a), where the amount of non-apatitic HPO_4^{2-} ions was clearly found to decrease for greater temperatures while the opposite trend was noticed for (apatitic) OH^-.

The temperature at which the maturation step is undergone is thus a second synthesis parameter playing a major role on nanocrystalline apatite physico-chemistry, producing an acceleration of the maturation process leading to chemical compositions closer to stoichiometry. Interestingly, the measure (after cooling) of the pH of the medium after maturation at increasing temperatures in the range 20–100 °C showed a decrease from pH = 7.2 to 6.8, and this slight acidification can indeed be related to the increased hydroxylation of the apatite phase, attributed to a promoted maturation (which consumes OH^- ions from the solution) when the apatite is subjected to higher temperatures.

At this stage, it was then interesting to follow cumulative effects of maturation time and temperature, and to draw some comparative assessments. In this case, comparisons were made for samples matured between 20 min and 1 week, and for temperatures between 20 and 50 °C, as these four limits appear as reasonable "extreme" values that may be encountered in real situations, in either

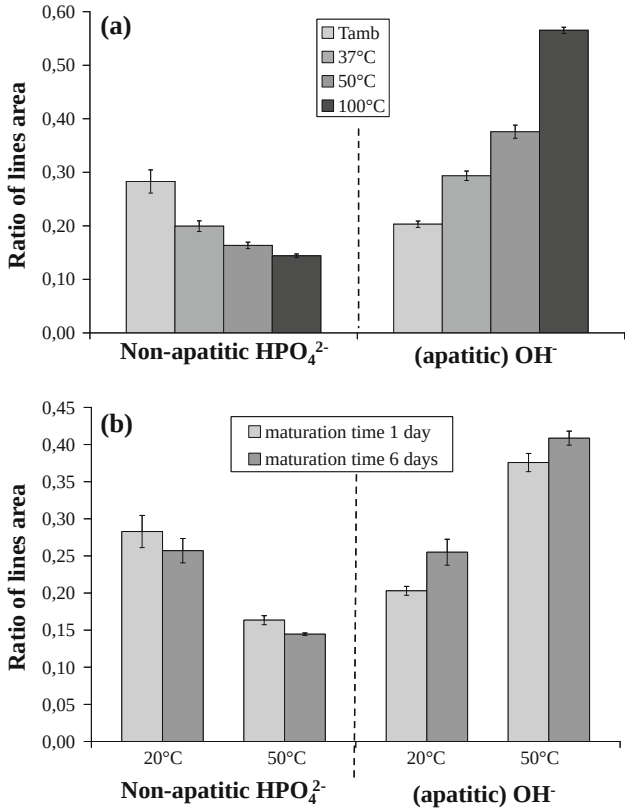

Fig. 8 Evolution of non-apatitic HPO_4^{2-} and (apatitic) OH^- ratios of *lines* area (based on FTIR decompositions) for **a** increasing maturation temperatures (for 1 day) and **b** cumulative maturation and temperature effects

laboratories or in the industry, for the preparation of such nanocrystalline apatites. Figure 8b reports for example the relative IR intensities of non-apatitic HPO_4^{2-} bands and (apatitic) OH^- bands, in the cases of samples matured for 1 or 6 days, at either 20 or 50 °C. As can be seen on this figure, although cumulative temperature and time effects are evidenced the effect of a change in temperature from 20 to 50 °C is significantly more pronounced than the effect of an increase in maturation time from 1 to 6 days.

These findings may thus find a direct echo for the industrial production of such nanocrystalline apatites, since they unveil the major impact of maturation temperature.

3.2.3 Effect of synthesis pH

Another generally important synthesis parameter in aqueous precipitation routes is the pH at which the precipitation takes place. Indeed, a change in pH of the precipitating medium is bound to lead to modifications of ionic speciation in solution. Typically, for calcium phosphate apatite precipitation, the relative amounts of ions such as PO_4^{3-}/HPO_4^{2-}/$H_2PO_4^-$ as well as Ca^{2+}/$Ca(OH)^+$ and H^+/OH^-, among other ionic species, will directly be impacted by the pH value [39]. In order to follow the role of pH on the nature and physico-chemical features of the precipitated phase(s), synthesis experiments were carried out here at pH 6, 7.2, 8, 9, 10 and 11, keeping all other parameters constant (ambient temperature, 1 day of maturation).

Our observations showed that at pH 6 (acidic conditions), the precipitated phase corresponded to brushite ($CaHPO_4{\cdot}2H_2O$) rather than apatite, as witnessed by XRD and FTIR results (not shown here for the sake of brevity). The formation of brushite in acidic media containing calcium and phosphate species is not highly surprising: indeed, brushite becomes thermodynamically more stable than hydroxyapatite below pH 4 [39]. At pH 6, hydroxyapatite is the theoretically most stable phase, but the transient observation of brushite can be linked to kinetic aspects, especially in conditions (ambient temperature, short maturation time) which do not favor the obtainment of stoichiometric HA as is the case here.

In contrast, only an apatitic phase could be detected in this work for experiments run at pH 7.2 or above. An increase of the synthesis pH led to a modification in the FTIR spectral decomposition features in the 400–800 cm^{-1} range as shown in Fig. 9: the amount of non-apatitic HPO_4^{2-} ions was found to follow a decreasing trend while OH^- ions exhibited the opposite tendency. Some carbonation of the samples (reaching a maximum of about 3 wt%) was also evidenced by absorption bands in the range 1,370–1,550 cm^{-1}, which may be related to a modification of the speciation between HCO_3^- and CO_3^{2-} ions upon alkalinization of the medium. Taking into account the presence of carbonate ions in the solid phase, no obvious variation of the overall Ca/(P + C) content was noticed in this work (where C represents the carbonate content).

Nevertheless, contrarily to the results obtained with increasing maturation time or temperature, this decrease in non-apatitic HPO_4^{2-} content and the increase in (apatitic) OH^- content and Ca/P ratio were not followed by an improvement of the crystallinity state as indicated by XRD

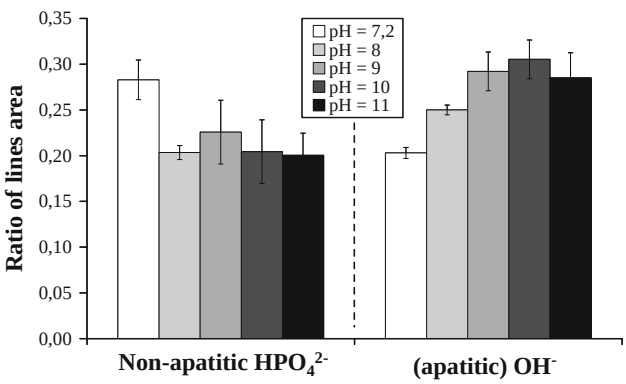

Fig. 9 Evolution of non-apatitic HPO_4^{2-} and (apatitic) OH^- ratios of lines area (based on FTIR decompositions) upon synthesis pH rise

Table 1 Evolution of mean crystallite lengths and widths upon pH increase from 7.2 to 11 (ambient temperature, 1 day of maturation)

	Mean crystalline length (based on Scherrer's formula) (nm)	Mean crystalline width (based on Scherrer's formula) (nm)	Mean crystalline length (based on Hosemann and Vogel's model) (nm)
pH = 7.2	19.4 ± 0.1	3.5 ± 0.1	14.7 ± 0.2
pH = 8	19.4 ± 0.1	4.1 ± 0.1	14.9 ± 0.8
pH = 9	16.0 ± 0.1	3.7 ± 0.1	12.7 ± 0.6
pH = 10	15.1 ± 0.1	3.4 ± 0.1	10.9 ± 0.1
pH = 11	15.0 ± 0.1	3.4 ± 0.1	13.6 ± 0.3

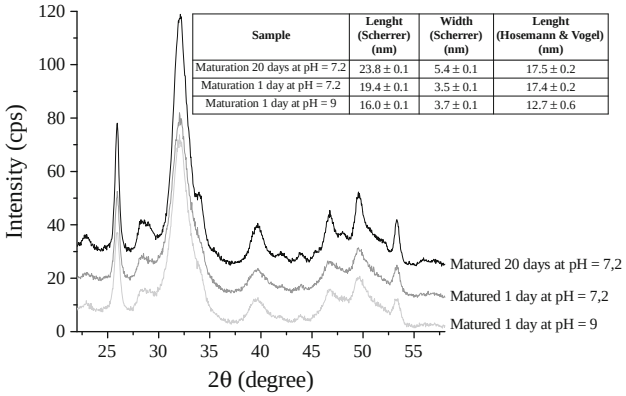

Fig. 10 Comparison of XRD features for apatites samples prepared at varying pH and maturation times (at room temperature)

data (not shown, accessible from the authors as additional resource). The estimation of mean crystallite dimensions by Scherrer's and Hosemann and Vogel's models then pointed out (Table 1) a slight decrease in mean length as the pH raised from 7.2 to 11 while crystallite mean widths did not change significantly. These findings may be linked to the increased supersaturation obtained upon pH raise, due to a progressive increase of the relative contents in PO_4^{3-} and OH^- ions [39]. In the precipitation process, this phenomenon may then favor the nucleation step at the expense of crystal growth, then ultimately leading to more numerous but smaller crystals. Another explanation for the obtainment of smaller crystals could be linked to the partial carbonation of the apatite obtained under alkaline pH, since carbonate ions are know as crystal growth inhibitor for apatite compounds [40, 41].

To illustrate those observations, a comparison with apatite compounds obtained with increasing maturation time (at pH = 7.2) can be made with the compounds obtained with varying pH. Based on chemical titration and FTIR spectral decomposition, the apatite compound synthesized at pH = 9 during a maturation time of 1 day was found to be close to the apatite sample prepared at pH = 7.2 for 20 days. Figure 10 reports the related XRD patterns, along with the reference compound prepared following the "reference" protocol. These data show that the duration of the maturation step during synthesis has a dominant effect on the crystallinity state of the precipitated apatite, as opposed to pH. However, pH remains a dominant parameter for the chemical composition of the precipitated phase.

3.2.4 Effect of the nature of starting phosphate salt

As the apatite structure can incorporate many substituents, the nature of counter-ions and impurities potentially contained in the starting salts used during synthesis may prove to have an impact on the physico-chemical features of the precipitate.

In order to shed some light on this matter, we studied here the influence of a change in the nature of phosphate salts, namely $(NH_4)_2HPO_4$ and Na_2HPO_4. To achieve a pertinent comparison between apatite compounds precipitated with $(NH_4)_2HPO_4$ and Na_2HPO_4, this study was undergone throughout the maturation timeframe ranging from 20 min to 20 days.

As for the precipitates obtained with $(NH_4)_2HPO_4$, the samples obtained with Na_2HPO_4 were found to consist in a single apatite phase as indicated by XRD analysis (accessible from the authors as additional resource). For each synthesis way, as maturation time increased, diffraction peaks became thinner and the resolution of the XRD patterns was significantly improved with time. As previously (see Sect. 3.2.1), such observations indicate intrinsic modifications in the apatite chemical (composition/stoichiometry) and/or physical features (crystallite size/internal constrains). However, some differences may be highlighted between apatite compounds synthesized with $(NH_4)_2HPO_4$ or Na_2HPO_4, for the same maturation time in solution. In particular, the XRD patterns obtained with sodium as counter-ion appeared to have a lower resolution than with ammonium, which is especially visible for the highest maturation time, despite crystallite lengths relatively close. This may be related to the possibility for sodium ions to enter rather easily the apatitic structure by substituting some calcium ions, while only very limited amounts of ammonium ions may be incorporated, especially for non-carbonated samples [42]. As the Na^+ ion possesses a single positive charge, compared to 2 positive charges for Ca^{2+}, Na^+ is then susceptible to cause some disturbances/microstrains in the apatitic lattice for charge balance (crystal overall electroneutrality), explaining the lower resolution of XRD patterns. Evaluations of the sodium content by ion chromatography indeed confirmed the incorporation of sodium, leading to Na/(Na + Ca) molar ratios between 2 and 7 mol.% for maturation times from 20 min to 20 days.

FTIR spectral decompositions in the 400–800 cm^{-1} range for both apatite compounds synthesized with

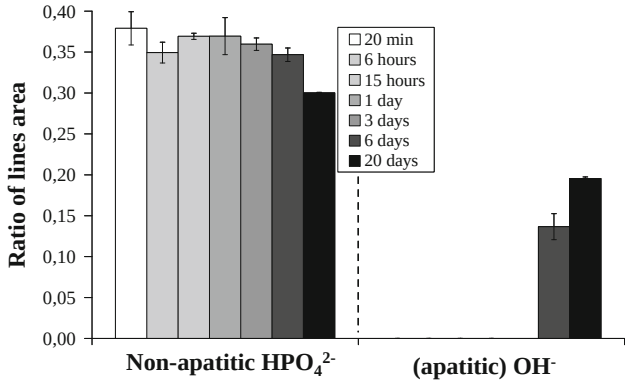

Fig. 11 Evolution of non-apatitic HPO_4^{2-} and (apatitic) OH^- ratios of lines area (based on FTIR decompositions) upon maturation time, for samples synthesized with Na_2HPO_4

$(NH_4)_2HPO_4$ and Na_2HPO_4 showed similar trends when maturation time increased, i.e. a progressive decrease with time of the non-apatitic HPO_4^{2-} content associated with an increase in apatitic OH^-. Nevertheless, these evolutions appeared delayed for samples containing Na^+ ions (Fig. 11) as compared to samples prepared with the ammonium phosphate salt (see Fig. 7): the decrease of the quantity of non-apatitic HPO_4^{2-} and the increase of (apatitic) OH^- indeed occurred only for maturation times greater than 3 days. In particular, for a given maturation time, the OH^- content was systematically lower in the presence of Na^+ than with ammonium. Moreover, chemical titrations led to lower Ca(+Na)/P global ratios for the sodium-containing samples (e.g. 1.43 ± 0.02 with sodium compared to 1.48 ± 0.02 with ammonium, for a maturation of 20 days). These observations may be related in part to the difference in charge between Na^+ and Ca^{2+} ions (the incorporation of monovalent Na^+ instead of bivalent Ca^{2+} requiring the reduction of the total amount of negative charges) possibly compensated for by the creation of OH^- vacancies.

These results therefore underline the necessity to be vigilant in the choice of starting salts when dealing with nanocrystalline apatite synthesis, since a great number of cations (but also anions) are susceptible to be incorporated into the apatitic lattice and thus to potentially modify the physico-chemical characteristics of such compounds.

3.3 Effect of post-treatments

3.3.1 Study of the immersion of freeze-dried apatite powder in aqueous medium

Taking into account the fact that apatite-based biomaterials will generally be employed by end-users in their dry state but for applications undergone in wet environments (e.g. in contact with body fluids, cell culture media etc.), it is relevant to examine the potential evolution endured by a dried nanocrystalline apatite powder upon (re)immersion in aqueous medium. A freeze-dried nanocrystalline apatite powder, synthesized following the "reference" protocol (corresponding to a maturation of 1 day at room temperature), was used as starting point in this study.

In a first step, two immersion solutions have been tested: an aqueous solution for which the pH was set to 7.2 by addition of a few drops of NaOH (0.05 M), and a phosphate solution (using $(NH_4)_2HPO_4$ 0.6 M) set to pH = 7.2 by addition of H_3PO_4: this second solution was selected in view of limiting the dissolution rate of the apatite phase during the test. The duration of this immersion step was fixed to 1 day for both solutions. Note that the presence of sodium from NaOH does not prove problematic here due to its low concentration, as its quantitative incorporation into the apatite phase would require significantly higher sodium concentrations (as suggested from our data presented in Sect. 3.2.4).

FTIR spectral decomposition results pointed out significant physico-chemical modifications in the ionic environments (Fig. 12) as compared to the reference sample: after immersion for 1 day in either of these two media, an important decrease of the non-apatitic HPO_4^{2-} content was indeed noticed, accompanied by an increase of (apatitic) OH^-. These observations are thus indicative of a modification of the crystals overall chemical composition due to this immersion treatment. These evolutions were also found to be associated to an improvement of the FTIR spectral resolution, which is especially noticeable in the $\nu_1(PO_4)$ region close to 961 cm^{-1} (not shown here), suggesting an enhancement of the global crystallinity state of the system.

Since this immersion step in aqueous medium is bound to allow additional "post-maturation" of the samples, a comparison to an apatite compound initially matured for

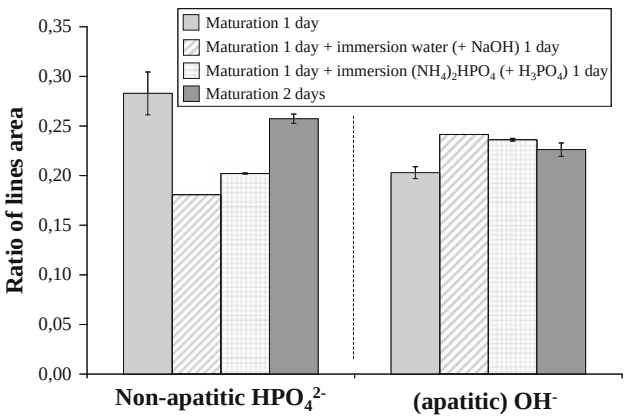

Fig. 12 Evolution of non-apatitic HPO_4^{2-} and (apatitic) OH^- ratios of lines area (based on FTIR decompositions) upon immersion in aqueous media of "reference" apatite powder, in comparison to freeze-dried apatite matured for 2 days

two consecutive days (thus presenting the same overall contact time between apatite nanocrystals and an aqueous medium) was carried out at this stage. Interestingly, FTIR results (Fig. 12) indicate that the impact on the physico-chemical features of apatite was amplified when an interruptive step was undergone, although no substantial difference was noticed between the two tested immersion media (see Fig. 12).

In order to inspect further these effects, additional experiments were carried out directly in the precipitation medium retrieved after filtration, and in water for comparison, on a reference apatite powder (1 day of maturation) immersed for a prolonged period of 10 days, and a sample matured for 11 consecutive days was also produced for comparison. In a similar way as above, the samples retrieved after this longer immersion period (independently of the two immersion solutions tested) were found to present altered physico-chemical features in comparison to the sample matured for 11 consecutive days. Chemical titrations indicated for instance a Ca/P molar ratio of 1.51 ± 0.02 for the samples freeze-dried and re-immersed, which proved to be greater than the value (1.49 ± 0.02) measured for the compound corresponding to 11 days of consecutive maturation. Surface Ca^{2+}/Mg^{2+} ion exchanges were also carried out on these various samples by soaking the powders in a Mg-rich solution (1 M). The amount of magnesium substituting surface calcium ions, as measured by atomic absorption, was close to 1.10 ± 0.10 wt% (namely 1.16 ± 0.11 and 1.07 ± 0.10 %) respectively for the sample re-immersed in the precipitating medium and in water, and this value was found to be lower than for the 11-day-matured sample (1.23 ± 0.11 wt% Mg). These findings thus indicate that the surface reactivity of re-immersed apatite samples was essentially retained, although a slight decrease in ion exchange ability may be suggested by these results (traduced here by a slight decrease of the amount of exchangeable (surface) calcium ions).

The above data enabled us to gather information on various effects due to the interruptive treatment prior to re-immersion of the powders in aqueous medium. In all cases, a comparison to samples which underwent a non-disrupted maturation in solution revealed (i) a slight decrease in the non-apatitic HPO_4^{2-} content, (ii) an increase in the amount of OH^- ions, (iii) a decrease in exchangeable surface Ca^{2+} ions, (iv) an increase in Ca/P molar ratio, and (v) an improvement of overall crystallinity state.

Since the nature of the re-immersion solution was found here to have only a limited impact on these parameters, the interruption of maturation seems to be chiefly at the origin of these effects, via freeze-drying and also possibly via its accompanying washing step: further studies will be needed to distinguish between those two phases of the interruptive process.

In previous studies [43, 44] we reported on a change in spectral features of nanocrystalline apatites upon drying, suggesting a partial denaturation of the non-apatitic hydrated layer on the surface of the nanocrystals. This phenomenon is schematized in Fig. 13. In this context, the evolutions of physico-chemical parameters observed in the present contribution after washing, freeze-drying and re-immersion may be linked to modifications of the surface characteristics of the nanocrystals implied by this interruptive process. Such a partial denaturation of the surface of the nanocrystals is likely to expose a greater amount of disorganized ions: upon re-immersion, part of these ions may then be more easily released in the surrounding solution. A possible reaction scheme may be found through the hydrolysis of PO_4^{3-} (and also possibly HPO_4^{2-}) ions such as:

$$PO^{3-}_{4\ \text{solid phase}} + H_2O \rightarrow HPO^{2-}_{4\ \text{solid phase}} + OH^-_{\text{solid phase}}$$

and/or

$$HPO^{2-}_{4\ \text{solid phase}} + H_2O \rightarrow H_2PO^{-}_{4\ \text{solid phase}} + OH^-_{\text{solid phase}}$$

followed by the release of calcium and hydrogenated phosphates ions into the solution through a surface reaction.

Upon re-immersion in water, this hypothesis could explain the decrease of non-apatitic HPO_4^{2-} ions and of exchangeable surface Ca^{2+} ions, and the increase of OH^- content in the apatite lattice. Moreover this phenomenon (which may be seen as some "leaching" effect of the surface of the nanocrystals) would then reduce the

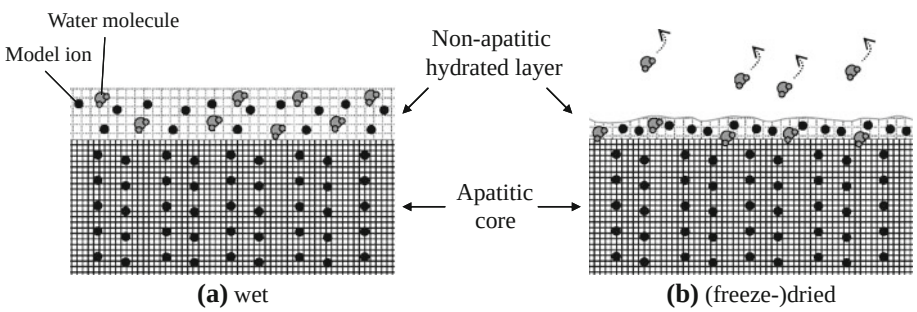

Fig. 13 Schematic view of the partial denaturation of nanocrystalline apatite hydrated layer upon (freeze-)drying

proportion of non-apatitic ionic environments relatively to the apatitic core, thus allowing an improvement of the overall crystallinity state of the system which was pointed out by a greater resolution of FTIR bands and X-Ray diffraction lines. It may however be inferred that, in the presence of an excess of phosphate ions in the re-immersion medium, the (persisting) presence of free calcium ions in solution is unlikely and reprecipitation phenomena may then come into play, thus leading to a more complex system that will need additional future investigations.

3.3.2 *Effect of thermal treatment of nanocrystalline apatite powders (dry state)*

Judging from the above results, nanocrystalline apatite physico-chemical features are revealed to be rather sensitive to several factors such as synthesis temperature or else the occurrence of a re-suspending step, among other parameters. In this context, it also appears interesting to evaluate the potential impact of a heat-treatment on the obtained dried samples. Therefore, we investigated here the effects of a thermal post-treatment of nanocrystalline apatite powders prepared by the "reference" synthesis protocol, at varying temperatures up to 100 °C which are bound to be used by experimentalists and/or apatite producers in their quest for biomimetic apatites potentially retaining their hydrated characteristic which was found to be of prime importance for surface reactivity.

XRD analyses indicated that the apatite phase was maintained after heat-treatment at 37, 50 and 100 °C for 3 days. The apatite crystallite dimensions derived from XRD pattern analysis were also found to be similar to those of the initial powder, with a mean length of 14.4 ± 0.2 nm (as estimated from Hosemann and Vogel's model) for T = 100 °C.

FTIR spectral decompositions performed on the apatite powders heat-treated for 3 days at 37, 50 and 100 °C showed however a decrease of non-apatitic HPO_4^{2-} content, associated with a decrease of apatitic OH^- as compared to the as-prepared (unheated) powder (Table 2). The overall amount of HPO_4^{2-} ions (both apatitic and non-apatitic) was also found to decrease, while the PO_4^{3-} content showed the opposite trend. These data suggest the deprotonation of some HPO_4^{2-} ions, which may then interact with OH^- ions so as to lead to the release of gaseous water through the reaction scheme:

$$HPO^{2-}_{4\ (\text{solid phase})} + OH^{-}_{(\text{solid phase})} \rightarrow PO^{3-}_{4\ (\text{solid phase})} + H_2O_{(\text{gas})}$$

In addition to this water release, arising from the elimination of some OH^- ions, part of the water molecules associated to the "hydrated" layer on the nanocrystals was also likely to be eliminated during the thermal post-treatment. It is however difficult, at this stage, to distinguish between those two types of released water molecules.

These findings are especially worth mentioning, taking into account the wide use of heating during some sterilization processes. Preliminary tests were then carried out here at 150 °C for 3 h., which corresponds to a heat treatment often encountered for sterilization in dry conditions (e.g. Pasteur oven). This treatment led, for an apatite sample (1 day of maturation) prepared with the "reference" protocol, to a weight loss of ca. 4.7 ± 0.4 wt%. Taking into account the conservation of a single apatite phase (as monitored by XRD and FTIR analysis), it is reasonable to attribute this weight loss to the release of water molecules due to exposure to 150 °C. These results thus point out a change in hydration state/composition of nanocrystalline apatite compounds when subjected to heat treatment, either for sterilization or during other processing steps. Although such modifications (which do not lead to a destruction of the apatite phase and nanocrystalline features) may remain acceptable for a variety of applications, their potential impact on the biomaterials characteristics should be carefully examined, as they may influence final in-use properties (e.g. cell–material interactions).

Table 2 Evolution of HPO_4^{2-}, PO_4^{3-}, and OH^- ratios of lines area (based on FTIR decompositions) upon thermal treatment of "reference" apatite powder, for 3 days at 37, 50 or 100 °C

	HPO_4^{2-} non-apatitic SD ± 0.02	HPO_4^{2-} apatitic	PO_4^{3-} total	OH^- (apatitic)
Reference powder	0.28	0.17	0.85	0.20
37 °C	0.18	0.18	0.84	0.16
50 °C	0.18	0.16	0.86	0.16
100 °C	0.20	0.13	0.88	0.18

4 Concluding remarks

This study underlines the need to monitor carefully all synthesis and post-synthesis parameters when dealing with the production, sterilization or storage of nanocrystalline apatite-based biomaterials. A careful attention must in particular be paid to three essential parameters, namely: maturation time in solution (prior to washing/drying), maturation temperature, and pH. Also, post-treatment processes such as sterilization by heat or re-immersion in aqueous media should be followed when setting up a production protocol, as the conditions of such post-treatments may lead to an often disregarded evolution or modification of the physico-chemical characteristics of the

initial samples. This contribution stresses the possibility to prepare highly-reactive biomaterials based on nanocrystalline apatite compounds; however it points out the need to control each step in production and storage processes.

Acknowledgments Part of this work was financially supported by the Agence Nationale de la Recherche in the scope of the ANR PICF 2009 "BioCapabili" project.

References

1. Rey C, Combes C, Drouet C, Glimcher MJ. Bone mineral: update on chemical composition and structure. Osteoporos Int. 2009;20: 1013–21.
2. Cazalbou S, Eichert D, Ranz X, et al. Ion exchanges in apatites for biomedical application. J Mater Sci Mater Med 2005;16: 405–409.
3. Legros R, Balmain N, Bonel G. Age-related-changes in mineral of rat and bovine cortical bone. Calcif Tissue Int. 1987;41: 137–44.
4. Neuman WF, Mulryan BJ. The surface chemistry of bone. IV. Further data on recrystallization. J Biol Chem. 1951;193:237–41.
5. Cazalbou S, Eichert D, Drouet C, et al. Biological mineralisations based on calcium phosphate. Comptes Rendus Palevol. 2004;3: 563–72.
6. Eichert D, Combes C, Drouet C, et al. Formation and evolution of hydrated surface layers of apatites. Bioceramics. 2005;17:3–6.
7. Eichert D, Salome M, Banu M, Susini J, Rey C. Preliminary characterization of calcium chemical environment in apatitic and non-apatitic calcium phosphates of biological interest by X-ray absorption spectroscopy. Spectrochim Acta B. 2005;60:850–8.
8. Rey C, Collins B, Goehl T, Dickson IR, Glimcher MJ. The carbonate environment in bone-mineral—a resolution-enhanced Fourier-transform infrared spectroscopy study. Calcif Tissue Int. 1989;45:157–64.
9. Young RA, Brown WE. Structures of biological minerals. In: Nancollas GH, editor. Biological mineralization and demineralization. Berlin: Springer; 1982. p. 101–41.
10. Eichert D, Drouet C, Sfihi H, Rey C, Combes C. Nanocrystalline apatite-based biomaterials: synthesis processing and characterization. In: Kendall JB, editor. Biomaterials research advances. New York: Nova Science Publishers; 2008. p. 93–143.
11. Rey C, Shimizu M, Collins B, Glimcher MJ. Resolution enhanced Fourier-transform infrared spectroscopy study of the environment of phosphate ions in the early deposits of a solid-phase of calcium-phosphate in bone and enamel, and their evolution with age. 1. Investigations in the HPO_4 domain. Calcif Tissue Int. 1990; 46:384–94.
12. Drouet C, Carayon M, Combes C, et al. Exchange of biologically relevant ions on nanocrystalline apatites. Geochim Cosmochim Acta. 2005;69:A69.
13. Drouet C, Carayon M, Combes C, et al. Surface enrichment of biomimetic apatites with biologically-active ions Mg^{2+} and Sr^{2+}: a preamble to the activation of bone repair materials. Mater Sci Eng C. 2008;28:1544–50.
14. Autefage H, Briand-Mesange F, Cazalbou S, Drouet C, Fourmy D, Goncalves S, Salles J, Combes C, Swider P, Rey C. Adsorption and release of BMP-2 on nanocrystalline apatite-coated and uncoated hydroxyapatite/beta-tricalcium phosphate porous ceramics. J Biomed Mater Res B. 2009;91B:706–15.
15. Ganesan K, Epple M. Calcium phosphate nanoparticles as nuclei for the preparation of colloidal calcium phytate. New J Chem. 2008;32:1326–30.
16. Lopez-Macipe A, Gomez-Morales J, Rodriguez-Clemente R. Nanosized hydroxyapatite precipitation from homogeneous calcium/citrate/phosphate solutions using microwave and conventional heating. Adv Mater. 1998;10:49–53.
17. Tas AC. Synthesis of biomimetic Ca-hydroxyapatite powders at 37 degrees C in synthetic body fluids. Biomaterials. 2000;21: 1429–38.
18. Chai CS, Ben-Nissan B. Bioactive nanocrystalline sol-gel hydroxyapatite coatings. J Mater Sci Mater Med. 1999;10:465–9.
19. Guo XY, Gough JE, Xiao P, Liu J, Shen ZJ. Fabrication of nanostructured hydroxyapatite and analysis of human osteoblastic cellular response. J Biomed Mater Res A. 2007;82A:1022–32.
20. Yeong KCB, Wang J, Ng SC. Mechanochemical synthesis of nanocrystalline hydroxyapatite from CaO and $CaHPO_4$. Biomaterials. 2001;22:2705–12.
21. Iafisco M, Delgado-Lopez JM, Gomez-Morales J, Hernandez–Hernandez MA, Rodriguez-Ruiz I, Roveri N. Formation of calcium phosphates by vapour diffusion in highly concentrated ionic micro-droplets. Cryst Res Technol. 2011;46:841–6.
22. Nassif N, Martineau F, Syzgantseva O, Gobeaux F, Willinger M, Coradin T, Cassaignon S, Azais T, Giraud-Guille MM. In vivo inspired conditions to synthesize biomimetic hydroxyapatite. Chem Mater. 2010;22:3653–63.
23. Phillips MJ, Darr JA, Luklinska ZB, Rehman I. Synthesis and characterization of nano-biomaterials with potential osteological applications. J Mater Sci Mater Med. 2003;14:875–82.
24. Thian ES, Ahmad Z, Huang J, Edirisinghe MJ, Jayasinghe SN, Ireland DC, Brooks RA, Rushton N, Bonfield W, Best SM. The role of electrosprayed apatite nanocrystals in guiding osteoblast behaviour. Biomaterials. 2008;29:1833–43.
25. Wu YQ, Hench LL, Du J, Choy KL, Guo JK. Preparation of hydroxyapatite fibers by electrospinning technique. J Am Ceram Soc. 2004;87:1988–91.
26. Sakhno Y, Bertinetti L, Iafisco M, Tampieri A, Roveri N, Martra G. Surface hydration and cationic sites of nanohydroxyapatites with amorphous or crystalline surfaces: a comparative study. J Phys Chem C. 2010;114:16640–8.
27. Drouet C, Bosc F, Banu M, et al. Nanocrystalline apatites: from powders to biomaterials. Powder Techol. 2009;190:118–22.
28. Vogel W, Hosemann R. Evaluation of paracrystalline distortions from line broadening. Acta Crystallogr A. 1970;26:272–7.
29. Kauppinen JK, Moffatt DJ, Mantsch HH, Cameron DG. Fourier self-deconvolution—a method for resolving intrinsically overlapped bands. Appl Spectrosc. 1981;35:271–6.
30. Fowler BO, Moreno EC, Brown WE. Infra-red spectra of hydroxyapatite, octacalcium phosphate and pyrolysed octacalcium phosphate. Arch Oral Biol. 1966;11:477–92.
31. Termine JD, Eanes ED, Greenfield DJ, Nylen MU, Harper RA. Hydrazine-deproteinated bone mineral. Physical and chemical properties. Calcif Tissue Res. 1973;12:73–90.
32. Kaflak A, Kolodziejski W. Complementary information on water and hydroxyl groups in nanocrystalline carbonated hydroxyapatites from TGA, NMR and IR measurements. J Mol Struct. 2011;990:263–70.
33. Charlot G. Chimie analytique quantitative, vol. 2. Paris: Masson; 1974.
34. Rowles SL. Studies on non-stoichiometric apatites. In: Fearnhead RW, Stack MV, editors. Tooth enamel Proc Int Symp. Bristol: John Wright & Sons; 1965. p. 23–25, 56–57.
35. Baig AA, Fox JL, Young RA, Wang Z, Hsu J, Higuchi WI, Chhettry A, Zhuang H, Otsuka M. Relationships among carbonated apatite solubility, crystallite size, and microstrain parameters. Calcif Tissue Int. 1999;64:437–49.
36. Handschin RG, Stern WB. X-ray diffraction studies on the lattice perfection of human bone apatite (*Crista iliaca*). Bone. 1995;16: S355–63.

37. Landis WJ, Hodgens KJ, Arena J, Song MJ, McEwen BF. Structural relations between collagen and mineral in bone as determined by high voltage electron microscopic tomography. Microsc Res Tech. 1996;33:192–202.
38. Cazalbou S, Combes C, Eichert D, Rey C, Glimcher MJ. Poorly crystalline apatites: evolution and maturation in vitro and in vivo. J Bone Miner Metab. 2004;22:310–7.
39. Elliott JC. Structure and chemistry of the apatites and other calcium orthophosphates, studies in inorganic chemistry, vol. 18. Amsterdam: Elsevier; 1994.
40. Barralet J, Best S, Bonfield W. Carbonate substitution in precipitated hydroxyapatite: an investigation into the effects of reaction temperature and bicarbonate ion concentration. J Biomed Mater Res. 1998;41:79–86.
41. Blumenthal NC, Betts F, Posner AS. Effect of carbonate and biological macromolecules on formation and properties of hydroxyapatite. Calcif Tissue Res. 1975;18:81–90.
42. Vignoles M, Bonel G, Young RA. Occurrence of nitrogenous species in precipitated B-type carbonated hydroxyapatites. Calcif Tissue Int. 1987;40:64–70.
43. Rey C, Combes C, Drouet C, al. e. Nanocrystalline apatites in biological systems: characterisation, structure and properties. Materialwiss Werkst 2007;38:996.
44. Rey C, Combes C, Drouet C, et al. Physico-chemical properties of nanocrystalline apatites: implications for biominerals and biomaterials. Mater Sci Eng C. 2007;27:198–205.